

# Temperature and voltage dependence of barrier height and ideality factor in Au/0.07 graphene-doped PVA/n-Si structures

S Altındal Yerişkin<sup>1</sup>, M Balbaşlı<sup>1</sup> and S Demirezen<sup>2\*</sup>

<sup>1</sup>Department of Chemical Engineering, Faculty of Engineering, Gazi University, Ankara, Turkey

<sup>2</sup>Department of Computer Aided Design and Animation, Vocational School of Design, Amasya University, Amasya, Turkey

Received: 07 March 2016 / Accepted: 16 September 2016 / Published online: 9 January 2017

**Abstract:** In this study, Au/0.07 graphene-doped PVA/n-Si structures were fabricated and current conduction mechanism in these structures were investigated in the temperature range of 80–380 K through forward bias current–voltage (*I*–*V*) measurements. Main electrical parameters were extracted from *I*–*V* data. Zero-bias barrier height ( $\bar{\Phi}_{B0}$ ) and ideality factor (*n*) were found strong functions of temperature and their values ranged from 0.234 eV and 4.98 (at 80 K) to 0.882 eV and 1.15 (at 380 K), respectively.  $\Phi_{ap}$  versus  $q/2kT$  plot was drawn to obtain an evidence of a Gaussian distribution of the barrier heights (BHs) and it revealed two distinct linear regions with different slopes and intercepts. The mean values of BH ( $\Phi_{B0}$ ) and zero-bias standard deviation ( $\sigma_s$ ) were obtained from the intercept and slope of the linear regions of this plot as 1.30 eV and 0.16 V for the first region (280–380 K) and 0.74 eV and 0.085 V for the second region (80–240 K), respectively. Thus, the values of  $\bar{\Phi}_{B0}$  and effective Richardson constant ( $A^*$ ) were also found from the intercept and slope of the modified Richardson plot [ $\ln(I_s/T^2) - q^2\sigma_s^2/2k^2T^2$  vs  $q/kT$ ] as 1.31 eV and 130 A/cm<sup>2</sup> K<sup>2</sup> for the first region and 0.76 eV and 922 A/cm<sup>2</sup> K<sup>2</sup> for the second region, respectively. The value of  $A^*$  for the first region was very close to the theoretical value for n-Si (112 A/cm<sup>2</sup> K<sup>2</sup>). The energy density distribution profile of surface states ( $N_{ss}$ ) was also extracted from the forward bias *I*–*V* data by taking into account voltage dependent effective BH ( $\Phi_e$ ) and *n*.

**Keywords:** Polymers; Electrical characteristics; Surface properties; Current-transport mechanisms

**PACS Nos.:** 73.20.-r; 73.40.-c; 73.30.+y

## 1. Introduction

Metal–semiconductor (MS) structures are known as Schottky barrier diodes/contacts (SBDs) and they are used in electronic and optoelectronic applications quite often. The electrical characteristics of a metal–semiconductor (MS) structure can be modified by using polymers and polymer composites; such as polyaniline, perylene, polypyrrole, polyvinyl alcohol (PVA) and graphene (GP), as interfacial layer material. Such interfacial layer is preferred in SBDs because it has several advantages and technical importance such as their flexibility, low cost production, good performance, low molecular weight, large area of production and easy processing compared to conventional inorganic based technologies [1–16]. PVA can be

considered as the most interesting material due to its large scale electronic and optoelectronic applications. It is well known SiO<sub>2</sub> serves as a good insulator for gate dielectric because of its good electrical properties, repeatability and process compatibility. On the other hand, conventional SiO<sub>2</sub> has unacceptably large leakage current. Therefore, especially in the last decade, many studies focus on how to improve device performance via growing new organic materials as interfacial layer [5–14]. Although, the polymer is a poor conductor, its conductivity can be improved by use of a metal or GP [4–6, 10, 11, 13, 15]. The main advantage of such interfacial layer at M/S interface is not only to realize the modification and continuous control of the BH but also the decrease in the magnitude of surface states ( $N_{ss}$ ), leakage current and series resistance ( $R_s$ ), whereas increasing rectification rate (RR) and shunt resistance ( $R_{sh}$ ) of the structure [1, 5, 6, 14].

\*Corresponding author, E-mail: selcukdemirezen@gmail.com

Graphene is a two dimensional (2D) layer of  $sp^2$ -bonded carbon material. It is a promising material in various fields owing to its extraordinary high specific surface area, excellent electric conductivity and superior mechanical stability [17, 18]. Recently, Schottky interfaces between GP and semiconductor are of interest for future applications in the electronic devices such as high speed logic gates, photo detector, three-terminal transistor [19, 20]. Usually, the value of barrier height represents the difference between work function of GP ( $\Phi_{GP}$ ) which is varied from 4.4 to 4.8 eV and electron affinity of Si ( $\chi$ ) [20]. GP also has a tunable band-gap, high transparency in visible range, high efficiency, low cost, high carrier mobility of  $15,000 \text{ cm}^2/v \text{ s}$ , high mechanical strength and it can be produced in the form of a ultrathin sheet as single layer or multilayers. Moreover, environmental friendly feature of GP also makes it an attractive material for electronic field. Due to extraordinary properties of it, GP nano sheets are ideal candidates for thin films and making combination with semiconductor materials [8, 17–20]. Very recently, Kaya et al. [21] showed that the value of dielectric constant ( $\epsilon'$ ) of graphene oxide (GO)-doped PrBaCoO nanoceramic at 1 kHz is almost 197 times greater than that of conventional  $\text{SiO}_2$ . It showed that high value of capacitance can be supplied by doping appropriate amount of GP or GO to nanoceramic or PVA materials at M/S interface instead of conventional low-dielectric interfacial insulator layer such as  $\text{SiO}_2$ . Therefore such doping procedure is expected to reveal high quality MPS structures.

Generally, the performance of structures of the SBD type (MS, MIS/MPS and solar cells) is dependent on surface preparation, sample temperature, interfacial layer (native or deposited), interface states which localized at M/S interface, applied bias voltage and barrier homogeneity. Particularly, variance of temperature and voltage has important effects on main diode parameters such as barrier height ( $\Phi_B$ ),  $n$  and  $N_{ss}$ . The important ones in these kind of structures are especially BH and  $n$  and their relationship. Because current transport from the interface between metal and semiconductor has a great sensitivity to barrier formation. In addition, the literature has shown that the analysis of the forward bias  $I$ - $V$  characteristics of SBD parameters only at room temperature does not provide detailed information about their conduction process or the nature of current conduction mechanism and barrier formation at M/S interface [3–6, 10–16]. Moreover, the temperature dependence of the  $I$ - $V$  measurements in a wide temperature range allows us to understand different aspects of current conduction process such as thermionic emission (TE), field emission (FE), recombination-generation (RG), interface recombination tunneling, minority carrier injection and tunneling via interface states or dislocations and Gaussian distribution in BH [22–26].

The first aim of this study is to fabricate a Au/0.07 GP-doped PVA/n-Si (MPS) type structures, rather than a classic metal-insulator-semiconductor (MIS) type structures, to improve the performance of structure for obtaining low surface states ( $N_{ss}$ ), leakage current and series resistance ( $R_s$ ). The second aim is to determine the possible current-conduction mechanisms in these structures in the wide temperature range of 80–380 K, by using the forward bias  $I$ - $V$  measurements. BH,  $n$  and other device parameters are found strong functions of temperature due to typical inhomogeneities in the distribution of BH at M/S interface. Experimental results show that GP-doped PVA interlayer may be a better candidate than other insulating materials in the future.

## 2. Experimental details

Au/0.07 GP-doped PVA/n-Si (MPS) type SBDs were fabricated on n-Si wafers with 5.08 cm diameter, (100) orientation, 350  $\mu\text{m}$  thickness and  $4.3 \times 10^{15} \text{ cm}^{-3}$  concentration of phosphor atoms. The wafer was first dipped in ammonium peroxide for 40 s to remove any native oxide layer on the surface and then was etched in sequence with acid solutions ( $\text{H}_2\text{SO}_4:\text{H}_2\text{O}_2:\text{H}_2\text{O} = 3:1:1$ ) for 60 s, and ( $\text{HCl}:\text{H}_2\text{O} = 1:1$ ) for another 60 s. The wafer was then rinsed in deionized water with high resistivity of 18  $\text{M}\Omega$  for a prolonged time and then dried in nitrogen gas. After that, high purity Au (99.995%) was thermally evaporated from the tungsten filament on the whole back side of the wafer at  $10^{-6}$  Torr in a metal evaporation system so that layer thickness is  $\sim 1500 \text{ \AA}$ . In order to obtain the low resistivity ohmic back contact, Au coated n-Si wafer was sintered at 500  $^\circ\text{C}$  for 5 min in nitrogen atmosphere.

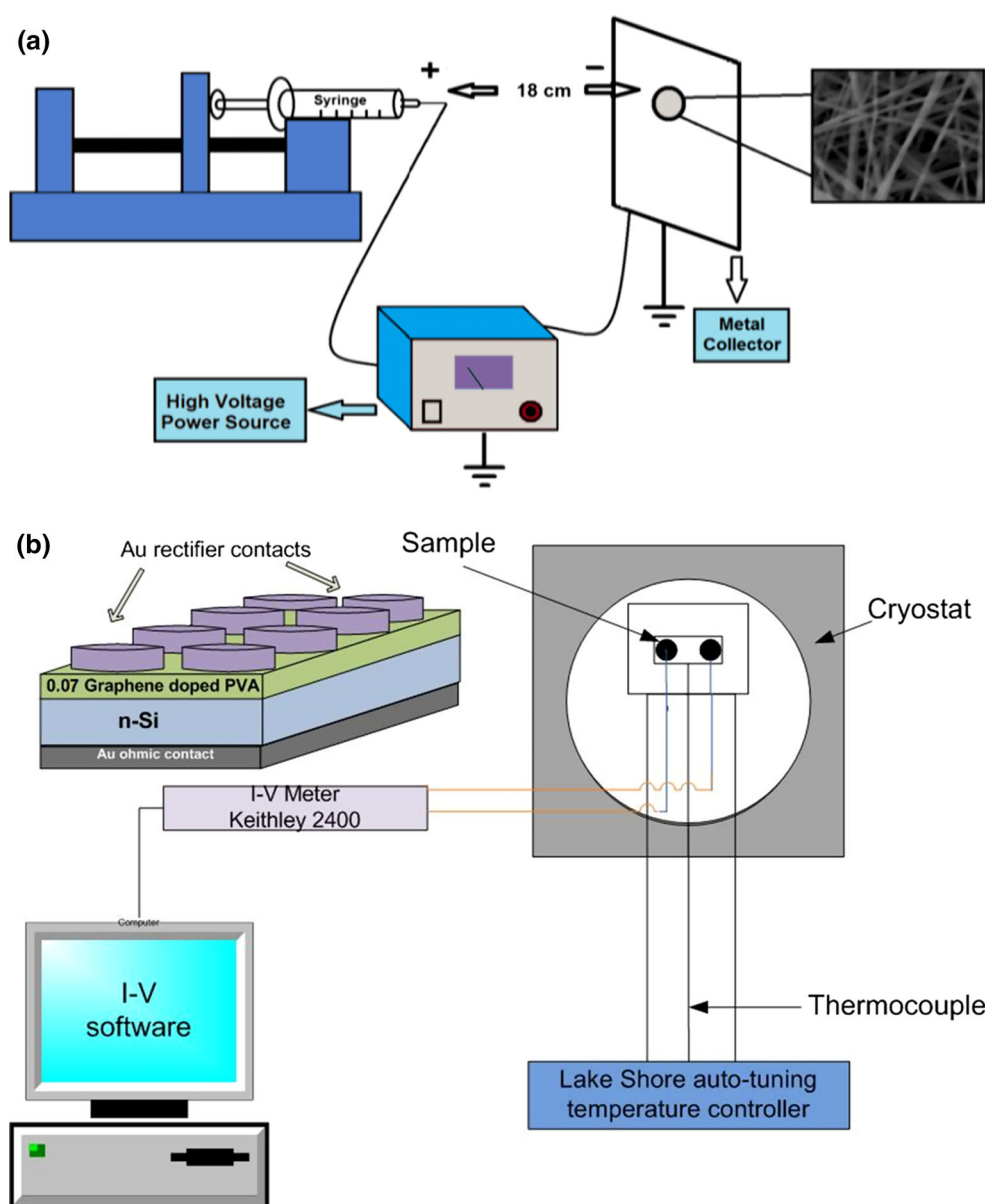
After formation of the ohmic contact, polyvinyl alcohol (PVA-Mw 130,000 g/mol) (Sigma-Aldrich) was used as the polymeric precursor. The thickness of GP (Grafen Chemical Industries Co) was 5–8 nm. Ultrapure deionized water which was produced by Millipore water and acetic acid (100%, Merck) was used as solvent. 7% GP powder was added to PVA powder. Firstly, the PVA solution (8% w/w) with deionized water was prepared by dissolving the PVA powder in ultrapure distilled and deionized water and heating the mixture up to 80  $^\circ\text{C}$  while stirring for 3 h. It was then cooled to room temperature. After that, GP solution (1.6% w/w) in  $N,N$ -dimethyl-formamide was prepared by treating it in Ultrasonic Shaker (BandelinSonorex, Berlin) for 48 h. PVA solution (8% w/w) and GP solution was then mixed at room temperature in order to obtain the process medium to be used in electro-spinning system. Finally, the wafer was pasted on a metal collector and the solution of nanosize PVA/GP compound was coated on the wafer through electro-spinning for

10 min. The distance between the wafer and the syringe (polymer hybrid solution) was adjusted to 18 cm and the voltage of 17 kV was applied to the solution at a flow rate of 0.5 ml/h. Thus, nano-fibers were attached to the wafer. The electro-spinning system consisted of a direct current (DC) high-voltage power supply (Gamma High Voltage Research, Inc., Ormond Beach, FL, USA; ES 30P-20 W/DAM), a dosing pump (New Era Syringe Pump), a plastic capillary tube (syringe), and a metal collector. The syringe was filled with polymer solution before the copper pins were connected to the power supply. The schematic diagram of the “Electrospinning system” is given in Fig. 1(a). Finally, circular dots with  $7.85 \times 10^{-3} \text{ cm}^2$  area and 1500 Å thick high purity Au rectifying contacts were deposited on the front side of the wafer through a metal

shadow mask at  $10^{-6}$  Torr. The schematic diagram of the Au/0.07 GP-doped PVA/n-Si structures and measurement system were given in Fig. 1(b). The samples were mounted on a Cu holder with a silver dag and electrical contact to the upper electrodes was made through thin silver coated Cu wires.

Au/0.07 GP-doped PVA/n-Si (MPS) type SBDs were then placed in a Janis vpf-475 cryostat, which allows measurements in the temperature range of 77–450 K. Then, the forward and reverse bias  $I$ - $V$  measurements were performed using a Keithley 2400 source meter in the temperature range of 80–380 K. The sample temperature was always monitored by using a Lake Shore model 321 auto-tuning temperature controllers with sensitivity better than  $\pm 0.1$  K. All measurements were carried out with the

**Fig. 1** (a) The schematic diagram of electrospinning system. (b) The schematic diagram of Au/0.07 GP-doped PVA/n-Si structure and measurement system



help of a microcomputer through an IEEE-488 AC/DC converter card.

### 3. Result and discussion

The forward and reverse bias semi-logarithmic  $I$ - $V$  characteristics of the Au/0.07 GP-doped PVA/ $n$ -Si structure between 80 and 380 K are shown in Fig. 2. As can be seen in Fig. 2, the value of current increases with increasing temperature in both reverse and forward biases. When the temperature increases, more and more electrons gain sufficient thermal energy to surmount the lowered patches of BH which occurs due to thermal expansion of the energy band and this leads to an increase in the current [22, 27–31]. However, the forward bias  $I$ - $V$  characteristics are linear on a semi-logarithmic scale at low forward bias voltages but this linearity deviates at high forward bias voltages due to the effect of  $R_s$ . Usually, at temperatures above room temperature and at low current levels, the thermionic emission theory (TE) is dominant current conduction mechanism. Otherwise at low temperatures the possible current-conduction mechanisms are more complicated [27]. Because, at low temperatures, the BH is lowered due to the patches or pinch-off around the mean BH [27]. Therefore, at the same forward bias, the current increases with increasing temperature. However, at higher forward biases, the effect of  $R_s$  is significant in the non-

linear region and this results in the reduction of the linear range of forward  $I$ - $V$  curves [28].

Also, the non-saturation behavior is observed (Fig. 2) as a function of the reverse bias. This behavior may be due to the reduction terms of the spatial inhomogeneity of SBH [29], and the image force lowering of SBH [28, 29]. When the diode has a series resistance ( $R_s$ ) and  $n$  is greater than unity, the relationship between current and applied voltage ( $V \geq 3kT/q$ ), according to the TE mechanism, can be given by [25, 26]

$$I = \underbrace{AA^*T^2 \exp(-q\Phi_{Bo}/kT)}_{I_s} \left[ \exp\left(\frac{q(V - IR_s)}{nkT}\right) - 1 \right] \quad (1)$$

where, the pre-factor is the reverse saturation current ( $I_s$  or  $I_o$ ) and  $A$ ,  $A^*$ ,  $\Phi_{Bo}$ ,  $V$ ,  $T$ ,  $k$ ,  $n$ ,  $IR_s$  are the diode area, effective Richardson constant for  $n$ -type Si ( $112 \text{ A/cm}^2\text{K}^2$ ) [25], zero-bias BH, applied bias voltage, absolute temperature in K, Boltzmann's constant, ideality factor and the voltage drop due to  $R_s$ , respectively. The  $n$  and  $I_s$  values are determined from the slope and intercept of the linear regions of  $\ln I$  versus  $V$  plot (Fig. 2) using Eq. (1) for each temperature level. The value of  $\Phi_{Bo}$  is calculated using theoretical value of  $A^*$  ( $112 \text{ A/cm}^2\text{K}^2$ ) and extrapolated  $I_s$  for each temperature level according to [25, 29]

$$\Phi_{Bo} = \frac{kT}{q} \ln\left(\frac{AA^*T^2}{I_s}\right) \quad (2)$$

The temperature dependent  $I_s$ ,  $n$ ,  $\Phi_{Bo}$  and  $n\Phi_{Bo}$  values are determined from the  $I$ - $V$  plots of Au/0.07 GP-doped PVA/ $n$ -Si structure and given in Table 1. As can be seen in Table 1 and Fig. 3,  $n$  and  $\Phi_{Bo}$  values of Au/0.07 GP-doped PVA/ $n$ -Si structure are strongly dependent on temperature and they ranged from 4.98 and 0.234 eV (at 80 K) to 1.15

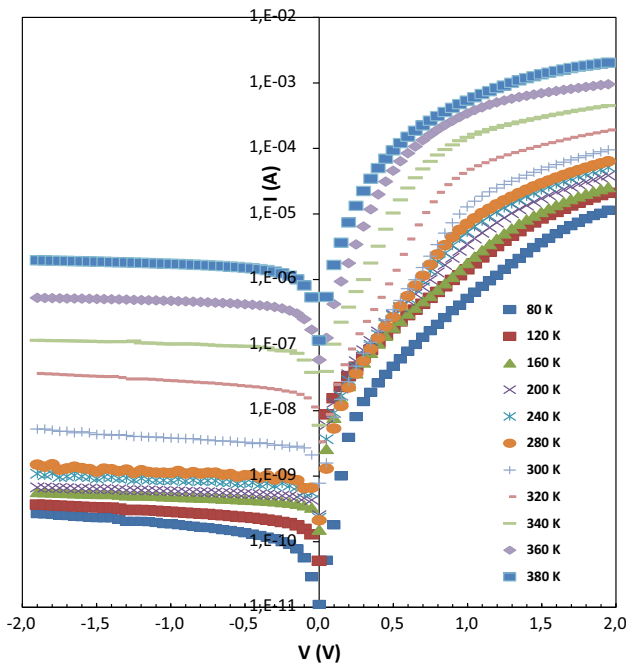


**Fig. 2** Forward and reverse bias semi-logarithmic  $I$ - $V$  characteristics of Au/0.07 graphene-doped PVA/ $n$ -Si structure at various temperatures

**Table 1** Temperature dependent values of various parameters determined from forward bias  $I$ - $V$  characteristics of Au/0.07 GP-doped PVA/ $n$ -Si structure

$T$ (K)	$I_s$ (A)	$n$	$\Phi_{Bo}$ (eV)	$nT$ (K)
80	1.10E-11	4.98	0.234	398.40
120	3.83E-11	3.36	0.346	403.01
160	9.37E-11	2.42	0.457	387.77
200	1.69E-10	1.97	0.569	393.20
240	2.87E-10	1.74	0.679	418.23
280	5.44E-10	1.53	0.784	427.07
300	1.31E-09	1.43	0.821	427.96
320	5.20E-09	1.27	0.841	406.54
340	1.49E-08	1.27	0.867	432.10
360	4.59E-08	1.19	0.886	427.96
380	2.58E-07	1.15	0.882	437.00

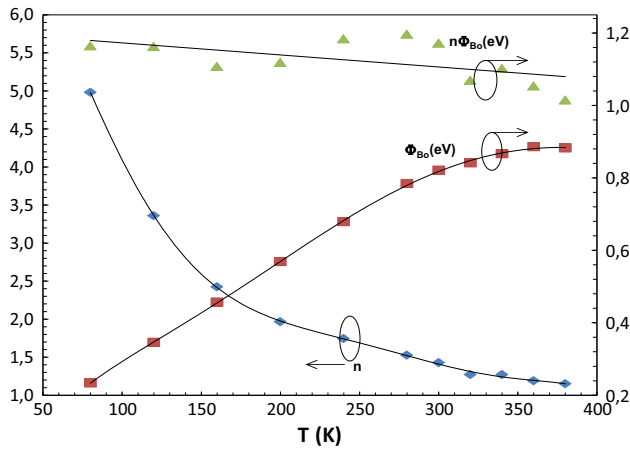


**Fig. 3** The temperature dependence of  $n$  and  $\Phi_{Bo}$  of Au/0.07 GP-doped PVA/n-Si structure obtained from the forward bias I–V data

and 0.882 eV (at 380 K), respectively. The value of  $n$  decreases with increasing temperature and such behavior is in agreement with literature. The high value of  $n$  at low temperatures can be attributed to the existence of insulator layer, image force lowering, density distribution of the interface states or interface traps ( $N_{ss}$  or  $D_{it}$ ) at M/S interface, and barrier inhomogeneity [27–33]. On the other hand,  $\Phi_{Bo}$  of Au/0.07 GP-doped PVA/n-Si structure exhibits an unusual behavior in a way that it increases with increasing temperature. Such temperature dependence is in obvious disagreement with the reported negative temperature coefficient of the barrier height or forbidden band gap of a semiconductor ( $\alpha_{Si} \approx -3.4 \times 10^{-4} \text{ eV K}^{-1}$ ) [25]. Also, such behavior of  $n$  and BH with temperature can be interpreted on the basis of the existence of GD of the BHs around a mean value of BH due to barrier inhomogeneities at M/S interface [27–31]. In this case, the current across the barrier can be greatly influenced due to barrier inhomogeneities.

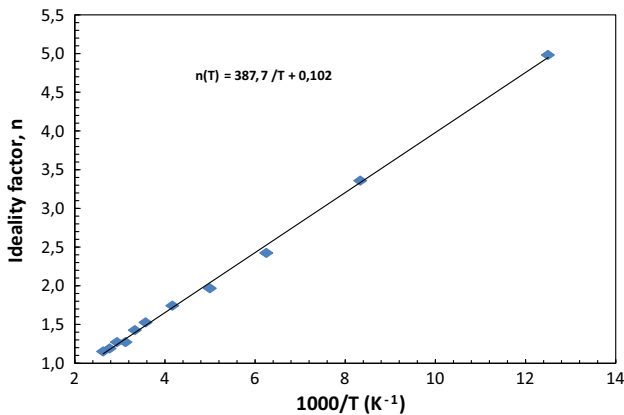


**Fig. 4** The plot of  $n$  versus  $1000/T$  of Au/0.07 GP-doped PVA/n-Si structure

As can be seen in Table 1 and Fig. 4,  $n$  is found to change linearly with temperature as below;

$$n(T) = n_o + \frac{T_o}{T} \quad (3)$$

where  $n_o$  and  $T_o$  are constants which are found to be 0.102 and 387.7 K, respectively.

The temperature dependent ideality factor is further analyzed by plotting  $n \cdot kT/q$  versus  $kT/q$  in order to obtain information on the main carrier transport mechanism in the SBD.  $n \cdot kT/q$  versus  $kT/q$  plot is given in Fig. 5, which shows the experimental and theoretical results together. It is clear that there is a correlation between the experimental and the theoretical curves ( $n \cdot kT/q$  vs  $kT/q$ ) for the sample. In this perspective, the straight line fit of the experimental values for the  $T_o$  effect should be parallel to that of the ideal Schottky contact behavior. As can be seen in Fig. 5, the straight line fit of the experimental values is not parallel to that of the ideal Schottky contact behavior. This is explainable in terms of SBH inhomogeneity.

The energy density distribution of the interface states ( $N_{ss}$ ) in equilibrium with the semiconductor can be determined from the forward bias I–V data by taking the voltage dependent ideality factor  $n(V)$  and effective barrier height ( $\Phi_e$ ) into account. The quantities of  $n(V)$  and ( $\Phi_e$ ) can be described by following equations, respectively [26].

$$n(V) = \frac{q}{kT} \left[ \frac{(V - IR_S)}{\ln(I/I_o)} \right] = 1 + \frac{\delta}{\epsilon_i} \left[ \frac{\epsilon_s}{W_D} + qN_{ss}(V) \right] \quad (4)$$

$$\Phi_e = \Phi_{Bo} + \beta(V - IR_S) = \Phi_{Bo} + \left( 1 - \frac{1}{n(V)} \right) (V - IR_S) \quad (5)$$

where  $\beta [=d\Phi_e/dV = 1 - 1/n(V)]$  is the voltage coefficient of the effective barrier height  $\Phi_e$ , which is used in place of the barrier height  $\Phi_{Bo}$ , and it is a parameter that includes

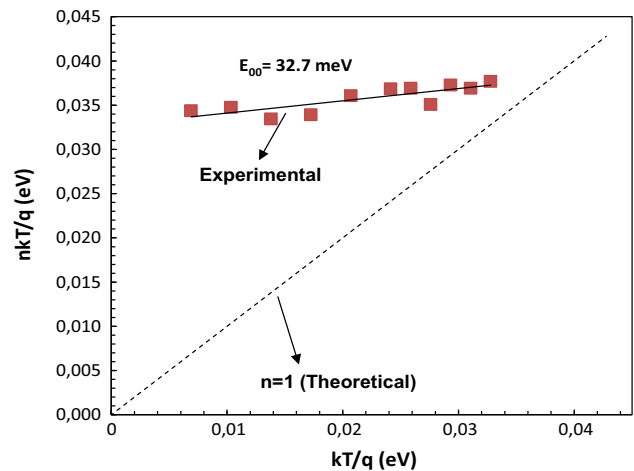


**Fig. 5** The plots of  $n \cdot kT/q$  versus  $kT/q$  of Au/0.07 GP-doped PVA/n-Si structure

the effects of interface states in equilibrium with the semiconductor. Density of interface states proposed by Card and Rhoderick can be simplified and given as [26]:

$$N_{ss}(V) = \frac{1}{q} \left[ \frac{\varepsilon_i}{\delta} (n(V) - 1) - \frac{\varepsilon_s}{W_D} \right] \quad (6)$$

where  $\delta$  is the thickness of interfacial insulator layer,  $W_D$  is the depletion layer width,  $\varepsilon_i = 4\varepsilon_0$ ,  $\varepsilon_s = 11.8\varepsilon_0$  are permittivity of the interfacial insulator layer and the semiconductor, respectively, and  $\varepsilon_0$  is the permittivity of the free space. The value of  $W_D$  is obtained from the experimental  $C^{-2}$ - $V$  plot for each temperature level at 1 MHz. Furthermore, for the n-Si, the energy dependent value of the  $N_{ss}$  with respect to the top of the conduction band ( $E_c$ ) at the surface of semiconductor is given as:

$$E_c - E_{ss} = q(\Phi_e - V) \quad (7)$$

Figure 6, shows the energy density distribution profile of the  $N_{ss}$  as a function of  $E_c - E_{ss}$  obtained from forward bias I-V characteristics. As can be seen in the figure, the value of  $N_{ss}$  exponentially grows from mid-gap of Si towards the bottom of conduction band. The obtained value of  $N_{ss}$  is on the order of  $\sim 10^{13} \text{ eV}^{-1} \text{ cm}^{-2}$  and can be considered suitable for a semiconductor device.

### 3.1. Inhomogeneous barrier analysis

For the evaluation of the BH, one may also make use of the Richardson plot of saturation current. In Eq. (1), the  $I_s$  can be re-organized as below;

$$\ln\left(\frac{I_s}{T^2}\right) = \ln(AA^*) - \frac{q\Phi_{Bo}}{kT} \quad (8)$$

where  $A$  is the diode area,  $A^*$  is the effective Richardson constant, and  $k$  is the Boltzmann constant. The

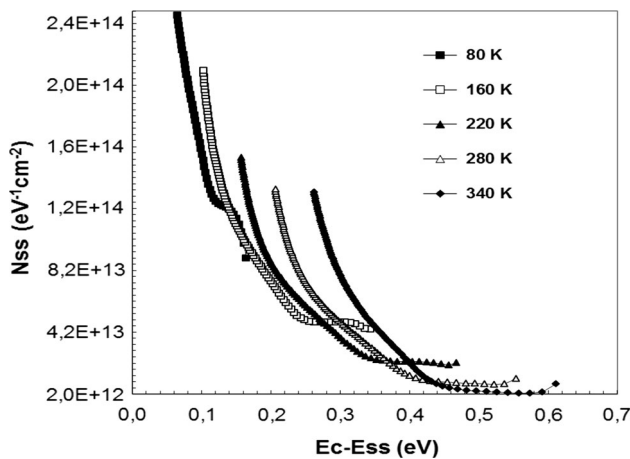


**Fig. 6** The energy distribution profile of the  $N_{ss}$  obtained from the forward bias I-V characteristics of Au/0.07 GP-doped PVA/n-Si structure at different temperature levels

conventional  $\ln(I_s/T^2)$  versus  $q/kT$  plot of Au/0.07 GP-doped PVA/n-Si structure is given in Fig. 7.

The conventional  $\ln(I_s/T^2)$  versus  $q/kT$  plot shows two linear regions with different slopes. Such behavior of Richardson plot can be attributed to the spatially inhomogeneous BHs and potential fluctuations at the interface or two distinct conduction mechanisms [29, 33–36]. As can be seen, the  $\ln(I_s/T^2)$  versus  $q/kT$  plot shows two distinct linear regions with different slopes and intercepts. In the first region (280–380 K), the values of the activation energy ( $E_a = \text{BH}$ ) and  $A^*$  are obtained from the slope and intercept of this straight-line as 0.496 eV and  $5.01 \times 10^{-4} \text{ A/cm}^2 \text{ K}^2$ , respectively, whereas they are obtained as 0.0109 eV and  $1.03 \times 10^{-12} \text{ A/cm}^2 \text{ K}^2$ , respectively, for the second region (80–240 K). It is well known, this value of  $A^*$  is much lower than the theoretical value of  $112 \text{ A/cm}^2 \text{ K}^2$  for n-Si. Fig. 8 consists two BHs which correspond to the low and high barrier areas. That is, at low temperatures, the carrier transport across MS contact would be preferentially through the lower barriers in the potential distribution [29, 36–39]. Horvath [33] explained that the  $A^*$  value obtained from the temperature dependent I-V characteristics may be affected by the lateral inhomogeneity of the barrier. Schmitsdorf et al. [34] used Tung's [27] theoretical approach and found a linear correlation between experimental zero bias BH and ideality factor.

As can be seen in Fig. 8, there is a linear correlation between  $\Phi_{Bo}$  and  $n$ . Similar results have been reported in the literature by Schmitsdorf et al. [34] and by Tung's [27] theoretical approach. They associated such behavior with the lateral inhomogeneities of the BHs. In the first region (280–380 K), the extrapolation of the experimental  $\Phi_{Bo}$  and  $n$  plot for  $n = 1$  reveals the value of 0.94 eV. In the second region (80–240 K), the extrapolation of the  $\Phi_{Bo}$  and

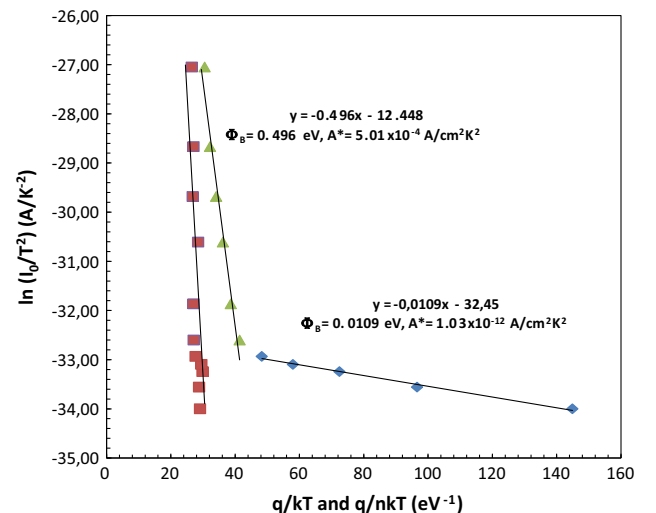


**Fig. 7** Richardson plots of the  $\ln(I_s/T^2)$  versus  $q/kT$  of Au/0.07 GP-doped PVA/n-Si structure

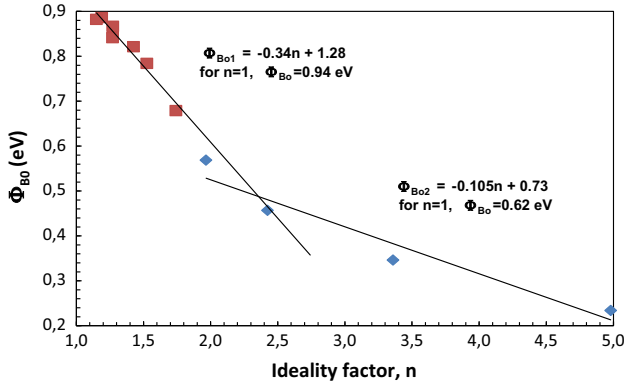


**Fig. 8**  $\Phi_{B0}$  versus  $n$  plot for Au/0.07 GP-doped PVA/n-Si structure

$n$  plot for  $n = 1$  reveals the value of 0.62 eV. Thus, it can be said that the decrease in the zero-bias BH and increase in the  $n$  especially at low temperatures are possibly caused by the BH inhomogeneities.

For the analysis based on barrier inhomogeneity, we adopted the model of Werner and Güttler [31], introducing a GD in the BH with a mean value  $\overline{\Phi}_{B0}$  and standard deviation  $\sigma_s$ .

$$P(\Phi_B) = \frac{1}{\sigma_s \sqrt{2\pi}} \exp \left[ -\frac{(\Phi_B - \overline{\Phi}_{B0})^2}{2\sigma_s^2} \right] \quad (9)$$

where  $1/[\sigma_s(2\pi)^{1/2}]$  is the normalization constant of the Gaussian BH distribution. The total  $I(V)$  across a SBD containing barrier inhomogeneities can be expressed as

$$I(V) = \int_{-\infty}^{+\infty} I(\Phi_B, V) P(\Phi_B) d\Phi, \quad (10)$$

where  $I(\Phi_B, V)$  is the current at a bias ( $V$ ) for a BH based on the ideal thermionic-emission-diffusion (TED) theory and  $P(\Phi_B)$  is the normalized distribution function giving the probability of accuracy for BH. Performing this integration from  $-\infty$  to  $+\infty$ , one can obtain the current  $I(V)$  through a SBD at a forward bias  $V$  as

$$I_s = AA * T^2 \exp(-q\Phi_{ap}/kT) \quad (11)$$

$$I(V) = AA * T^2 \exp \left[ -\frac{q}{kT} \left( \overline{\Phi}_{B0} - \frac{q\sigma_0^2}{2kT} \right) \right] \times \exp \left( \frac{qV}{n_{ap}kT} \right) \left[ 1 - \exp \left( -\frac{q(V - IR_s)}{kT} \right) \right], \quad (12)$$

where  $\Phi_{B0}$  and  $n_{ap}$  are the apparent barrier height and apparent ideality factor, respectively and are given by [26, 29]

$$\Phi_{ap} = \Phi_{B0}(T = 0) - \frac{q\sigma_0^2}{2kT}, \quad (13)$$

$$\left( \frac{1}{n_{ap}} - 1 \right) = \rho_2 - \frac{q\rho_3}{2kT} \quad (14)$$

It is assumed that the modified SBH  $\overline{\Phi}_{B0}$  and  $\sigma_s$  have linear dependence on Gaussian parameters which are bias dependent. Such dependence is given by  $\overline{\Phi}_B = \overline{\Phi}_{B0} + \rho_2 V$  and standard deviation  $\sigma_s = \sigma_{s0} + \rho_3 V$ , where  $\rho_2$  and  $\rho_3$  are voltage coefficients which may depend on temperature and they quantify the voltage deformation of the BH distribution [31]. The temperature dependence of  $\sigma_s$  is usually small and can be neglected [33–36].

As can be seen in Fig. 9(a), the plot of  $\Phi_{ap}$  versus  $q/2kT$  shows two distinct linear regions with different slopes and intercepts. In the first region (280–380 K), the values  $\Phi_{B0}$  and zero bias standard deviation ( $\sigma_s$ ) are obtained from the intercept and slope of this straight-line as 1.30 eV and 0.16 V, respectively, whereas they are obtained as 0.74 eV and 0.085 V, respectively, in the second region (80–240 K). Such behavior of the double GD is also reported in literature [26, 35, 36]. These changes are attributed to the chemical treatment of the semiconductor surface [37, 38]. Likewise, as also indicated by Chand and Kumar [39], the existence of a double GD in the M/S contacts can be attributed to the nature of the inhomogeneities themselves in the two cases. This may involve variation in the interface composition, interface quality, electrical charges and non-stoichiometry, etc. Similarly, as can be clearly seen in Fig. 9(b), the plot of  $(n_{ap}^{-1} - 1)$  versus  $q/2kT$  should also possess different characteristics in the two temperature ranges because of the diode contains two BH distributions. The values of  $\rho_2$  are obtained from the intercepts of the experimental  $(n_{ap}^{-1} - 1)$  versus  $q/2kT$  plot as  $-0.08$  V in 280–380 K range (the distribution 1) and  $-0.33$  V in 80–240 K range (the distribution 2). On the other hand, the values of  $\rho_3$  are obtained from the slopes as 0.034 V in 280–420 K range and 0.0068 V in 120–240 K range. The linear behavior of this plot demonstrates that  $n$  indeed expresses the voltage deformation of the GD of the SBH. As can be seen in the  $(n_{ap}^{-1} - 1)$  versus  $q/2kT$ ,  $\rho_3$  value or the slope of the distribution 1 is larger than that of the distribution 2, therefore we may point out that the distribution 1 has wider and relatively higher BH with bias coefficients  $\rho_2$  and  $\rho_3$  being smaller and larger, respectively. Thus, we can say that the distribution 2 at low temperatures may possibly arises due to some phase changes taking place on cooling below a certain temperature. There are two distinct straight lines with different slopes at above figures. These results show that the BH is dependent on temperature and two different current transport mechanisms or two different mean BHs may dominate in the related temperature range. As a result, the predominant current transport is not only TE and FE in our samples; rather, there are two Gaussian distributions; i.e. GD1 and GD2, of BHs in the constant area corresponding to the high and low temperature regions, respectively. Furthermore, the temperature range covered

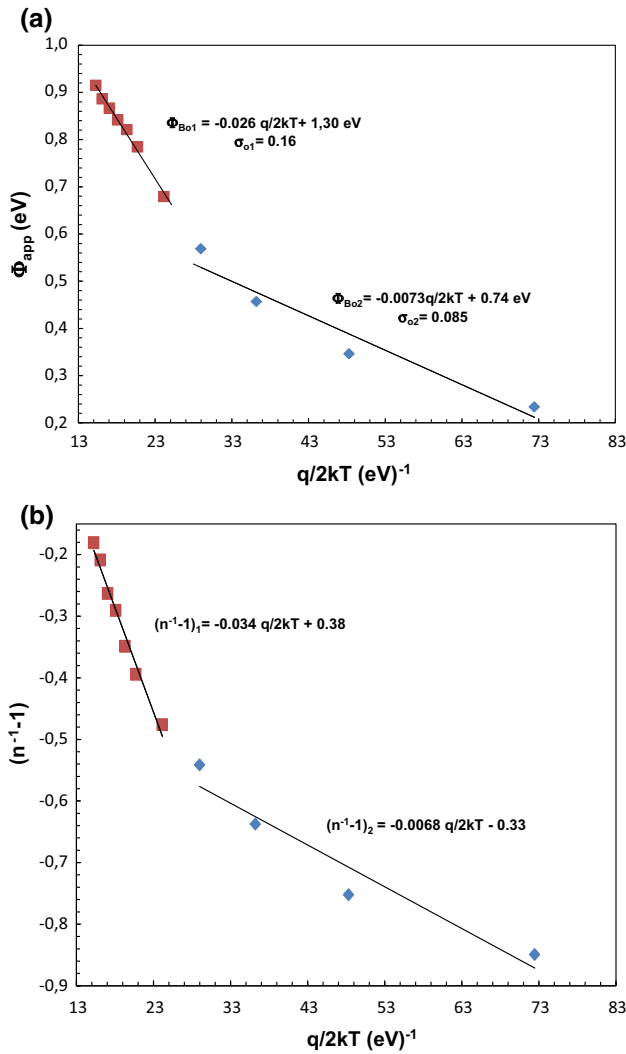


**Fig. 9** (a) The apparent BH [ $\Phi_{BO}$  ( $I$ - $V$ )] versus  $q/2kT$  plot and (b) the ideality factor ( $n^{-1} - 1$ ) versus  $q/2kT$  plot of Au/0.07 GP-doped PVA/n-Si structure

by each straight line suggests the regime where the corresponding distribution is effective [39]. It is believed that the barrier height (BH) differences over the Schottky contact area are due to inhomogeneous interfacial layer thickness and nature of BH, as well as non-uniformity of the interfacial charges or dislocations [40]. These results imply that the investigation of the electrical influence of the  $I$ - $V$  characteristics of the Schottky diodes is very important especially at low temperatures. Thus,  $I$ - $V$  measurements at very low temperatures make it possible to reveal the nature of barrier inhomogeneities present in the contact area [41–43].

As can be seen in Fig. 7, the conventional activation energy  $\ln(I_s/T^2)$  versus  $q/kT$  plot shows two linear regions. For explaining such discrepancy, Eqs. (8) and (13) are rewritten as below by taking into account the Gaussian

distribution of the BH and the modified Richardson or activation energy plot [27–31, 43–45].

$$\ln\left(\frac{I_s}{T^2}\right) - \left(\frac{q^2\sigma_o^2}{2k^2T^2}\right) = \ln(AA^*) - \frac{q\Phi_{Bo}}{kT} \quad (15)$$

Thus a modified activation energy plot from this expression is obtained. Using the experimental  $I_s$  data, a modified  $\ln(I_s/T^2) - q^2\sigma_o^2/2k^2T^2$  versus  $q/kT$  plot (Fig. 10) can be obtained using Eq. (15). This plot should reveal a straight line with slope directly yielding the mean  $\Phi_{Bo}$  and the intercept ( $=\ln AA^*$ ) at the ordinate determining  $A^*$  for a given diode area  $A$ . The  $\ln(I_s/T^2) - q^2\sigma_o^2/2k^2T^2$  values are calculated for two values of  $\sigma_s$ , obtained for the temperature ranges of 80–240 and 280–380 K. Fig. 10 shows the modified  $\ln(I_s/T^2) - q^2\sigma_o^2/2k^2T^2$  versus  $q/kT$  plots for both values of  $\sigma_s$ . The best linear fit of these modified experimental data is depicted by solid lines in Fig. 10 which represents the true activation energy plots in respective temperature range. The statistical analysis yielded zero bias mean BH  $\Phi_{Bo}$  as 0.76 eV (in the range 80–240 K) and 1.310 eV (in the range 280–380 K). These values match exactly with the mean BHs obtained from the  $\Phi_{ap}$  versus  $q/2kT$  plot in Fig. 9(a). The interceptions at the ordinate yield the Richardson constant  $A^*$  as 922 A/cm<sup>2</sup> K<sup>2</sup> (in 80–240 K range) and 130 A/cm<sup>2</sup> K<sup>2</sup> (in 280–380 K range) without using the temperature coefficient of the BHs. The value of the Richardson constant for 280–380 K range is very close to the theoretical value of 112 A/cm<sup>2</sup> K<sup>2</sup> for n-Si.

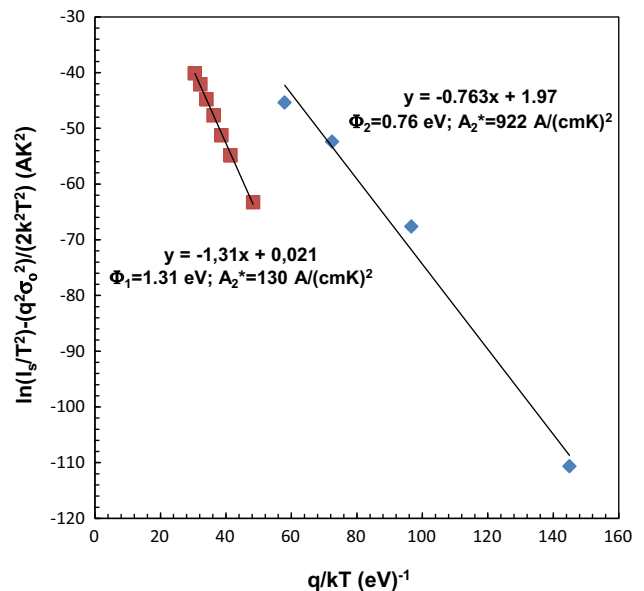


**Fig. 10** Modified Richardson  $\ln(I_s/T^2) - q^2\sigma_o^2/2k^2T^2$  versus  $q/kT$  plot of Au/0.07 GP-doped PVA/n-Si structure according to GD of BHs



#### 4. Conclusions

In this study the possible current-conduction mechanisms of Au/0.07 GP-doped PVA/n-Si structure were investigated in the wide temperature range of 80–380 K, by using the forward bias  $I$ - $V$  measurements. Experimental results showed that the values of zero-bias barrier height ( $\Phi_{B0}$ ) and ideality factor ( $n$ ) were strong functions of temperature and they ranged from 4.98 and 0.234 eV (at 80 K) to 1.15 and 0.882 eV (at 380 K), respectively, when these values were determined from standard Thermionic emission (TE) theory.  $\Phi_{ap}$  versus  $q/2kT$  plot was drawn to obtain an evidence of a Gaussian distribution (GD) of the barrier heights (BHs) and it showed two distinct linear regions with different slopes and intercepts. The mean values of BH ( $\Phi_{B0}$ ) and zero-bias standard deviation ( $\sigma_s$ ) were obtained from the intercept and slope of these plots as 1.30 eV and 0.16 V for the first region (280–380 K) and 0.74 eV and 0.085 V for the second region (80–240 K), respectively. Thus, the values of  $\bar{\Phi}_{B0}$  and effective Richardson constant ( $A^*$ ) were also obtained from the intercept and slope of the modified Richardson plot [ $\ln(I_s/T^2) - q^2\sigma_s^2/2k^2T^2$  vs  $q/kT$ ] as 1.31 eV and 130 A/cm<sup>2</sup> K<sup>2</sup> for the first region and 0.76 eV and 922 A/cm<sup>2</sup> K<sup>2</sup> for the second region, respectively. The value of  $A^*$  for the first region was very close to the theoretical value of 112 A/cm<sup>2</sup> K<sup>2</sup> for n-Si. The energy density distribution profile of surface states ( $N_{ss}$ ) was also extracted from the forward bias  $I$ - $V$  data by taking into account voltage dependent effective BH ( $\Phi_e$ ) and  $n$  for five different temperature level and growth from mid-gap of Si towards the bottom of conduction band was observed. The values of  $N_{ss}$  decreased with increasing temperature due to the restructure and reordering of them under temperature effect. In conclusion, the temperature dependence of the forward bias  $I$ - $V$  characteristics in the Au/0.07 GP-doped PVA/n-Si structures can be successfully explained with a double Gaussian distribution (DGD) of the BHs. We can say that GP-doped PVA interlayer may be a better candidate than other insulating materials in the future.

**Acknowledgements** This study was supported by Gazi University Scientific Research Project (Project number: GU-BAP.06/2016-13).

#### References

- [1] G D Sharma, S K Gupta and M S Roy *Thin Solid Films* **333** 176 (1998)
- [2] A Tombak, Y S Ocak, S Asubay, T Kılıçoğlu, F Özkahraman *Mater. Sci. Semicond. Proc.* **24** 187 (2014)
- [3] Ş Karataş and F Yakuphanoglu *Mater. Chem. Phys.* **138** 72 (2013)
- [4] H Uslu, Ş Altındal and İ Dökme *J. Appl. Phys.* **108** 104501 (2008)
- [5] Ş Altındal, T Tunç, H Tecimer and İ Yucedag *Mater. Sci. Semicond. Proc.* **28** 48 (2014)
- [6] İ M Afandiyeva, S Demirezen and Ş Altındal *J. Alloys Compd* **552** 423 (2013)
- [7] M Soylu, M Cavaş, A A Al-Ghamdi, Z H Gafer, F El-Tantawy and F Yakuphanoglu *Solar Energy Mater. Solar cell.* **124** 180 (2014)
- [8] H G Çetinkaya, S Alialy and Ş Altındal *J. Mater. Sci: Mater Electron* **26** 3186 (2015)
- [9] H Uslu, İ Dökme, İ M Afandiyeva and Ş Altındal *Surf. Interface Anal.* **42** 807 (2010)
- [10] S Demirezen, Ş Altındal and İ Uslu *Curr. Appl. Phys.* **13** 53 (2013)
- [11] İ Dökme and Ş Altındal *Fiber Poly.* **15** 2253 (2014)
- [12] Ö Güllü, M Çankaya, M Biber and A Türüt *J. Phys: Condens. Matter.* **20** 215210 (2008)
- [13] S Parui, R Ruitter, P J Zomer, M Wojtaszek, B J Van Wees and T Banerjee *J. Appl. Phys.* **116** 244505 (2014)
- [14] Ç Bilkan, S Zeyrek, S E San and Ş Altındal *Mater. Sci. in Semicond. Proc.* **32** 137 (2015)
- [15] H G Çetinkaya, H Tecimer, H Uslu and Ş Altındal *Curr. Appl. Phys.* **13** 1150 (2013)
- [16] S A Yeriskin, H İ Ünal and B Sarı *J. Appl. Polym. Sci.* **120** 390 (2011)
- [17] H S Soliman, A Faidah, Sh El-Ghamdy and A A Hindi *Phys. B Cond. Matter.* **406** 234512 (2011)
- [18] H Li, J Wei, Y Ojan, J Zhang, J Yu and G Wang *Colloids Surf. A: Physicochem. Eng. Asp.* **449** 148 (2014)
- [19] H Yang et al. *Science* **336** 1140 (2012)
- [20] M D Stoller, S Park, Y Zhu, J An, R S Ruoff *Nano Lett.* **8** 3498 (2008)
- [21] A Kaya, S Alialy, S Demirezen, M Balbaş, S A Yerişkin and A Aytumur *Ceram. Int.* **42** 322 (2016)
- [22] E Özavcı, S Demirezen, U Aydemir and Ş Altındal *Sens. Actuators: A Phys.* **194** 259 (2013)
- [23] E H Nicollian and A Goetzberger *Bell Syst. Tech. J.* **46** 1055 (1967)
- [24] E H Nicollian and J R Brews *MOS (Metal Oxide Semiconductor) Physics and Technology* (New York: Wiley) (1982)
- [25] S M Sze *Physics of Semiconductor Devices*, 2nd edn. (New York: Wiley) (1980)
- [26] H C Card and E H Rhoderick *J. Phys. D Appl. Phys.* **4** 1589 (1971)
- [27] R T Tung *Phys. Rev. B* **45** 13509 (1992)
- [28] P Chattopadhyay and D P Haldar *Appl. Surf. Sci.* **143** 287 (1999)
- [29] E H Rhoderick and R H Williams *Metal Semiconductor Contacts*, 2nd edn. (Oxford:Clarendon Press) (1988)
- [30] M K Hudait and S B Krupanidhi *Phys. B* **307** 125 (2001)
- [31] J H Werner and H H Güttler *J. Appl. Phys.* **69** 1522 (1991)
- [32] R Hackam and P Harrop *IEEE Trans. Electron Devices* **19** 1231 (1972)
- [33] Zs J Horvarth *Solid-State Electron* **39** 176 (1996)
- [34] R F Schmitsdorf, T U Kampen and W Mönch *Surf. Sci.* **324** 249 (1995)
- [35] A F Ozdemir, A Turut and A Kökçe *Semicond. Sci. Technol.* **21** 298 (2006)
- [36] H Tecimer, S Aksu, Y Atasoy, E Bacaksız and Ş Altındal *Sens. Actuators: A Phys.* **185** 73 (2012)
- [37] T U Kampen, S Park and D R T Zahn *Appl. Surf. Sci.* **190** 461 (2002)
- [38] A R V Roberts and D A Evans *Appl. Phys. Lett.* **86** 072105 (2005)
- [39] S Chand and J Kumar *Semicond. Sci. Technol.* **11** 1203 (1996)
- [40] N Tugluoglu, H Koralay, K.B. Akgül, Ş Çavdar, *Indian J. Phys.* **90** 43 (2016)

- 
- [41] V R Reddy *Indian J. Phys.* **89** 463 (2015)
- [42] D Sri Silpa, P Sreehith, V R Reddy and V Janardhanam *Indian J. Phys.* **90** 29 (2016)
- [43] S Altındal *J. Mater. Electron. Devices* **1** 42 (2015)
- [44] Y M Reddy, R Padmasuvarna, T L Narasappa, R Padma and V R Reddy *Indian J. Phys.* **89** 1161 (2015)
- [45] A Bobby, N Shiwakoti, P S Gupta and B K Antony *Indian J. Phys.* **90** 307 (2016)